Research Article | Vol. 10, No. 4 | 1 Apr 2019 | BIOMEDICAL OPTICS EXPRESS 1774
Biomedical Optics EXPRESS

Differentiating melanoma and healthy tissues based on elasticity-specific Brillouin microspectroscopy

MARIA TROYANOVA-WOOD,[1] ZHAOKAI MENG,[1] AND VLADISLAV V. YAKOVLEV[1,2,*]

[1]*Department of Biomedical Engineering, Texas A&M University, College Station, TX 77843-3120, USA*
[2]*Department of Physics, Zhejiang University, Hangzhou, Zhejiang 310027, China*
**yakovlev@tamu.edu*

Abstract: The main objective of the present study is to evaluate the use of Brillouin microspectroscopy for differentiation of melanoma and normal tissues based on elasticity measurements. Previous studies of malignant melanoma show that the lesion is stiffer than the surrounding healthy tissue. We hypothesize that elasticity-specific Brillouin spectroscopy can be used to distinguish between healthy and cancerous regions of an excised melanoma from a Sinclair miniature swine. Brillouin measurements of non-regressing and regressing melanomas and the surrounding healthy tissues were performed. Based on the Brillouin measurements, the melanomas and healthy tissues can be successfully differentiated. The stiffness of both tumors is found to be significantly greater than the healthy tissues. Notably, we found that the elasticity of regressing melanoma is closer to that of the normal tissue. The results indicate that Brillouin spectroscopy can be utilized as a tool for elasticity-based differentiation between malignant melanoma and surrounding healthy tissue, with potential use for melanoma boundary identification, monitoring tumor progression, or response to treatment.

© 2019 Optical Society of America under the terms of the OSA Open Access Publishing Agreement

1. Introduction

The ability of melanoma to spread throughout the body by reaching lymph or blood vessels makes it the deadliest of skin cancers [1]. While not as common as other cutaneous cancers, the incidence of malignant melanoma is on the rise, having increased by three times between 1970s and 2000s in the U.S [2], resulting in an estimated 9,940 fatalities within the last year [3]. Melanoma that is detected early can be successfully treated; however, with the progression of the disease, the mortality rate rapidly increases, reaching 94% in the distant stage [3]. The survival rate, therefore, greatly depends upon early diagnosis of the melanoma.

The location of the melanoma on the surface of the skin makes it visible and accessible, however, the diagnosis of this cancer is not simple. The appearance of malignant melanoma is similar to other pigmented skin lesions, both benign and malignant. Morphological features form the basis of most approaches to clinical diagnosis of melanoma. If initial evaluation suggests a possibility of melanoma, the biopsy of the lesion is taken for a histological verification of the diagnosis, which may take several days. The common diagnostic algorithm is evaluation of the lesion's asymmetry, border irregularity, color and diameter (ABCD). Most often the evaluation is achieved by naked-eye examination, the sensitivity of which is 85% [4]. Dermoscopy, or dermatoscopy, a technique with greater sensitivity and specificity of the diagnosis, utilizes a microscopic evaluation of the lesion's morphological features [5,6].

However, evaluation of morphological features is not the only method to diagnose malignant melanoma. A lot of research is conducted on methods that aim to increase the accuracy of melanoma diagnosis and aid pre-operative assessment of tumor margins and

#353347 https://doi.org/10.1364/BOE.10.001774
Journal © 2019 Received 5 Dec 2018; revised 19 Feb 2019; accepted 20 Feb 2019; published 11 Mar 2019

Biomedical Optics EXPRESS

thickness. Among them are conventional and high-frequency ultrasound [7–10], ultrasound elastography [9–11], multispectral imaging [12–14], MRI [15,16], and Raman spectroscopy [17–19].

Of particular interest is the diagnosis based on the change in the mechanical properties between malignant and healthy tissue or cells. The rigidity of many tumor types compared to the surrounding normal tissue is well known and is routinely used; a common example is palpation during breast cancer screening [20]. This variation in elasticity between the malignant mass and the normal tissue can be utilized to achieve a non-invasive diagnosis. One available elasticity-specific technique, ultrasound elastography [21], determines the elasticity score of the tissue by comparing measurements before and after applied compression. This method has been used to successfully discriminate between benign and malignant lesions in breast [22,23] and prostate [23], and it displayed potential in diagnosis of malignant melanoma [11]. However, ultrasound elastography measures the macroscopic elasticity, which often differs from the elasticity on a microscale [24–26]. For example, tumors are stiffer than healthy tissue on a macroscopic level, but individual cancerous cells of many cancer types are softer [27,28], which is related to their ability to invade and metastasize [29,30]. Interestingly, that is not always the case, and AFM elastography study on melanocytes has shown that pigmented human melanoma cells are stiffer than both healthy melanocytes and non-pigmented melanoma cells from same cell line [31]. Evaluating microelasticity instead of macroelasticity can be used to identify the tumor margin with high resolution, and can become a valuable tool for research of cancer progression. Brillouin spectroscopy can be used to probe the elastic properties of bulk tissue, while also providing an adequate spatial resolution to measure elasticity of individual cells.

Brillouin microspectroscopy is an emerging technique for measuring the viscosity and elasticity of a sample. Brillouin spectroscopy is based on the inelastic interaction of the incident photons and investigated material's spontaneous acoustic phonons. The incident wave undergoes a small, 1-10 GHz, change in frequency– called the Brillouin shift, which is related to the material's high-frequency elastic modulus. The Brillouin shift is equal to $\Delta\nu_B = \pm 2\frac{nV_s}{\lambda_0}\sin(\frac{\theta}{2})$, where n and V_s are the refractive index and the speed of sound in the material, λ_0 is the wavelength of the incident light and θ is the collection angle. The above equation can be used to directly calculate the speed of sound from the Brillouin shift. Assuming the collection angle of $\theta = \pi$, such as in the present study, the speed of sound is then calculated as: $V_s = \frac{\Delta\nu_B\lambda_0}{2n}$. Furthermore, the real part of the longitudinal modulus M' is related to the speed of sound and the material's mass density, ρ, as $M' = V_s^2\rho$. This relationship can be used to determine the longitudinal modulus from the Brillouin shift; for a signal collection limited to $\theta = \pi$ it is $M' = \frac{1}{4}\rho(\frac{\Delta\nu_B\lambda_0}{n})^2$.

Brillouin spectroscopy is a non-destructive and label-free approach to determining viscoelasticity of a wide range of materials. Brillouin spectroscopy has been successfully applied in recent years in a number of biological applications [32–40]. Brillouin spectroscopy nondestructively measures elasticity with high spatial resolution, making it a feasible method to differentiate between healthy tissue and tumors.

The animal model for malignant melanoma used in this study is Sinclair miniature swine. Sinclair miniature swine is an accepted model of human melanoma, first used in a study of malignant melanocytic tumors in 1974 [41]. These animals possess melanoma lesions at birth, or develop them within a few days after birth. These malignant lesions are histopathologically similar to human malignant melanoma, albeit with greater melanin concentration. However, the melanoma in Sinclair swine spontaneously regress within weeks, and new lesions do not

Biomedical Optics EXPRESS

form. A loss of pigmentation commonly accompanies the melanoma regression in the area surrounding the lesion, and is frequently present elsewhere on the body. The preliminary results of Brillouin spectroscopy measurements of Sinclair swine melanoma have been published by our group previously [42,43]. In the present study we have obtained multiple measurements from both a normal non-regressing melanoma and a regressing melanoma with a visible depigmentation around the primary lesion. We hypothesize that the elasticity of the regressing tumor will be close or equal to the elasticity of the surrounding healthy tissue, while the non-regressing melanoma will be the stiffest of the three sample types. It is worth noting that change in the Brillouin shift can be attributed to both change in tissue elasticity and refractive index. Melanocytes in non-regressing melanoma have a greater number of melanin granules within the cell than those in the normal tissue. The higher concentration of melanin would reflect in a higher absorption and refractive index of the lesion. At the same time, the higher melanin content in melanoma melanocytes has been shown to result in higher cell stiffness, measured with AFM elastography [31]. While it is impossible to state by what extent the increase in the Brillouin shift can be attributed to a change in stiffness alone, the conclusion that melanoma lesion is stiffer than surrounding normal tissue is supported by published literature, for example, the real-time tissue elastography study [11].

We hypothesize that Brillouin microspectroscopy can be used to distinguish malignant tumors from surrounding normal tissue. In this report, we demonstrate the application of this method on an animal model of malignant melanoma. We have successfully obtained Brillouin shift measurements from healthy, cancerous and regressing tissues and found the variations in the Brillouin shift between all three tissue types to be statistically significant.

2. Materials and methods

Melanoma samples

The samples of malignant melanoma, collected from Sinclair miniature swine, were kindly provided by Dr. D. Kraemer (College of Veterinary Medicine & Biomedical Sciences; Texas A&M University). All animal procedures were approved by our Institutional Animal Care and Use Committee and were in accordance with federal and local regulations. The melanomas with 2 cm margins were surgically removed from a 6-weeks old male Sinclair miniature swine under anesthesia. One of the lesions was identified as a non-regressing melanoma (Fig. 1(a)), circle marking the lesion), while the second tumor displayed depigmentation around the lesion, and was determined to be a regressing melanoma (Fig. 1(b), circle marking the lesion and arrow pointing to the area of depigmentation). The samples were placed in sealed containers filled with phosphate saline buffer (PBS) on ice, and the Brillouin measurements were obtained on the same day.

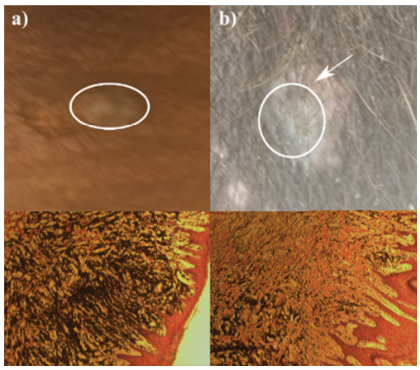

Fig. 1. Photos (top, circles mark the lesions, arrow points to the area of depigmentation) and corresponding histology slides of lesion cross-section (bottom, H&E stain) of: (a) normal non-regressing melanoma and (b) regressing melanoma.

Biomedical Optics EXPRESS

An average of 3 replicate Brillouin spectra from 8 different locations per tissue type were obtained from the central areas of the malignant growths and from the healthy tissue regions at a distance of 1 cm from the sample's edge. In the regressing melanoma sample, the healthy region was sampled away from the area of depigmentation. The integration time was 60 s and the incident power on the sample did not exceed 20 mW; no thermal damage to the sampled area was detected following the data collection.

Brillouin spectroscopy setup

Figure 2 shows the schematic diagram of the optical setup for Brillouin microspectroscopy, which followed our earlier design [44,45]. More detail on the system's latest design and performance is provided in Coker *et al*. [46].

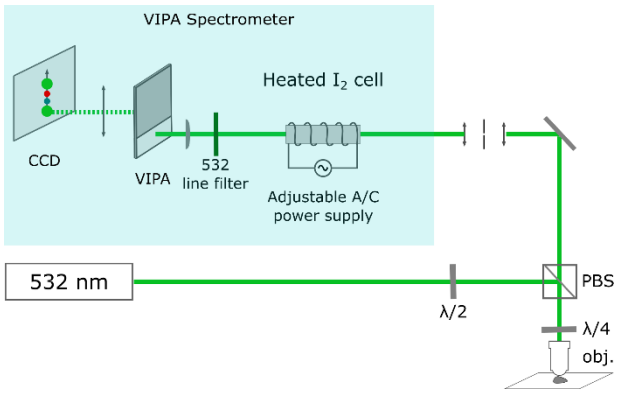

Fig. 2. Schematic diagram of instrumental setup for Brillouin spectroscopy. The heated iodine cell served as an ultra-narrow notch filter. Abbreviations: PBS – polarizing beamsplitter, obj. – 20x objective lens, λ/2 – half-wave plate and λ/4 – quarter-wave plate.

A 532-nm single- frequency laser (Lasermate Inc.; GMSL-532-100FHA) served as the source of the incident light. The incident light passed through a polarizing beamsplitter towards the infinity-corrected microscope objective lens (Nikon Inc., CFI Plan Fluor 20x, N.A. = 0.5), which both focused the incident light onto the sample, and collected the backscattered signal. A quarter-wave plate and the polarizing beamsplitter redirected the collected signal towards the VIPA spectrometer, with a pinhole placed before the spectrometer serving to reduce the amount of out-of-focus light reaching the detector. The VIPA spectrometer consisted of a temperature-tunable iodine absorption cell (Opthos Instruments, Inc.) set to 112°C which served as an ultra-narrow notch filter, and 532-nm line filter that filtered the undesired laser, Raman and I_2 fluorescence frequencies, followed by VIPA and the CCD.

3. Results and discussion

To illustrate typical raw and processed Brillouin spectra, an example from a single measurement of non-regressing and regressing melanomas, and the healthy tissue region is presented in Fig. 3(a). Notably, the SNR between the three spectra is different, even though the acquisition parameters remained unchanged. The healthy tissue possesses the greatest SNR, while the signal from the non-regressing melanoma has the smallest SNR. These differences in the signal quality is likely due to the increased absorption of the incident light by the melanin, the concentration of which is the greatest in the non-regressing melanoma. The Brillouin peaks are fit with the Lorentzian function to obtain their central frequency, as shown in Fig. 3(b). Both tumors and healthy tissue possess notably different Brillouin shifts; the results of all measurements (N = 8 per tissue type) are displayed as mean ± standard deviation in Fig. 4.

Biomedical Optics EXPRESS

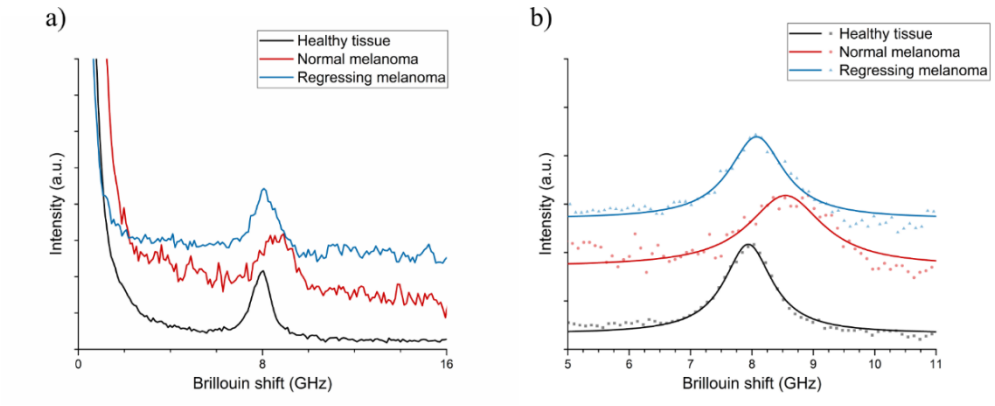

Fig. 3. Example Brillouin spectra, anti-Stokes Brillouin peaks of healthy tissue, normal non-regressing and regressing melanoma: (a) typical raw Brillouin spectra and (b) the expanded view showing the Lorentzian function fit of the data.

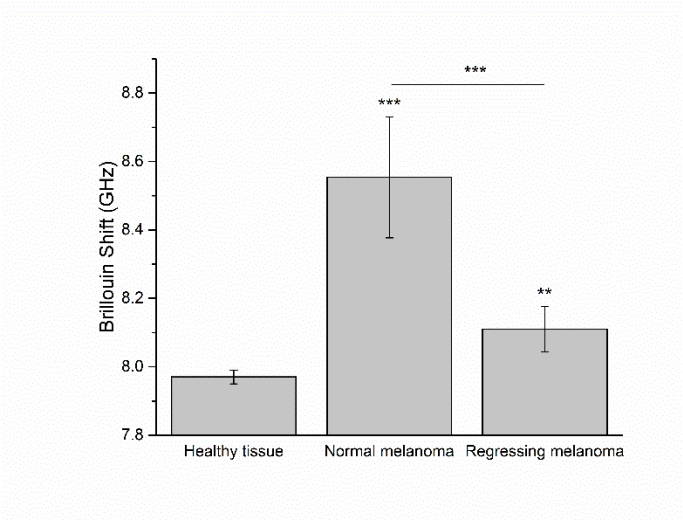

Fig. 4. Brillouin shifts of the healthy tissue, normal non-regressing and regressing melanomas, displayed as mean ± standard deviation. The difference between the Brillouin shifts is statistically significant (*** $p \leq 0.001$, ** $p \leq 0.01$).

One-way ANOVA test was used to compare the means of the Brillouin shift for all samples; the results of the statistical analysis show that the Brillouin shift is significantly different in both melanomas and the surrounding healthy tissue. The average Brillouin shifts are 8.55 ± 0.18 GHz (Normal non-regressing melanoma), 8.11 ± 0.07 GHz (Regressing melanoma), and 7.97 ± 0.02 GHz (Healthy tissue). Both melanoma lesions are stiffer than the surrounding normal tissue, which possesses the smallest value of the Brillouin shift. These results support the literature-based hypothesis that melanoma is stiffer than the healthy tissue. In the present study, the samples included both a non-regressing and a regressing melanoma, and the Brillouin shift shows variation between the two lesion types. The regressing melanoma possesses elasticity closer to that of the surrounding healthy tissue. In Sinclair swine, melanoma regression and loss of pigmentation is related to a rise in antibodies to antigens primarily expressed on melanocytes [47]. Early stage of regression is characterized by a decrease in active melanocytes and predominance of melanophages, while the final stage of regression is histologically similar to normal tissue [41]. The sample used in the present study was at an intermediate stage of regression, with bluish in color lesion and

Biomedical Optics EXPRESS

depigmentation halo surrounding it. The reduction in the number of melanocytes and increase in melanin-laden macrophages and T-lymphocytes at the site likely contribute to the decrease in stiffness of the regressing melanoma compared to the non-regressing melanoma.

The use of the 532-nm wavelength in the present study results in heating of the pigmented tissue due to absorption by melanin. No thermal damage to the sample was observed, however, in order to avoid the damage, the power of the incident radiation was set as low as feasible, which affected the signal to noise ratio of most of our Brillouin spectra. The lower power lead to a longer signal collection time, which, while acceptable for single-point measurements, would be impractical for larger number of data points in point-scanning mode. The present study of elasticity-specific Brillouin measurements of malignant melanoma will be continued; a future study will use Brillouin microspectroscopy to identify melanoma border with high precision by obtaining an elasticity map of the sample. In future studies, either a longer incident excitation wavelength, i.e. 780 nm, will be used to reduce the acquisition time, because the skin's absorption and heating generally declines within the 400-1064 nm range as wavelength increases [48,49], or nonlinear Brillouin microscopy measurements [50,51] will be adapted for those tissue measurements.

4. Conclusion

The ability of Brillouin spectroscopy to differentiate between malignant melanoma and surrounding healthy tissue was successfully demonstrated for the first time. The use of Sinclair miniature swine as an animal model of human malignant melanoma allowed for Brillouin shifts' comparison between the normal non-regressing melanoma, regressing melanoma and the surrounding healthy tissue. The Brillouin shifts of the samples are statistically significantly different, with the healthy tissue being the softest, and the non-regressing melanoma the stiffest sample.

In the present study, the Brillouin shift of the regressing melanoma differed from the measurements of both the non-regressing melanoma and the heathy tissue. Among the potential applications of Brillouin spectroscopy is not only differentiation between the cancerous and normal tissue, but also monitoring tumor progression or evaluation of treatment efficacy. These potential uses make Brillouin microspectroscopy a valuable tool in cancer research.

Brillouin microspectroscopy is uniquely suitable for distinguishing between different tissues or areas of a sample on the basis of differences in their elastic properties. Brillouin spectroscopy was successfully applied to distinguish between cancerous, regressing and healthy regions of melanoma samples based on their elasticity. This spectroscopic approach shows potential for differentiating malignant melanoma from other pigmented skin lesions, and for finding the boundaries of the lesion with high precision.

Funding

National Science Foundation (NSF) (DBI-1455671, DBI-1532188, ECCS-1509268, CMMI-1826078); Air Force Office of Scientific Research (AFOSR) (FA9550-15-1-0517, FA9550-18-1-0141); Defense Advanced Research Projects Agency (DARPA) (FA8650-13-D-6368/0006); Office of Naval Research (ONR) (N00014-16-1-2578); National Institute of General Medical Sciences (NIGMS) (1R01GM127696-01).

Disclosures

The authors declare that there are no conflicts of interest related to this article.

References

1. A. J. Miller and M. C. J. Mihm, Jr., "Melanoma," N. Engl. J. Med. **355**(1), 51–65 (2006).
2. C. Garbe and U. Leiter, "Melanoma epidemiology and trends," Clin. Dermatol. **27**(1), 3–9 (2009).
3. American Cancer Society, "American Cancer Society: cancer facts and figures 2015," (2015).
4. C. M. Grin, A. W. Kopf, B. Welkovich, R. S. Bart, and M. J. Levenstein, "Accuracy in the clinical diagnosis of

Biomedical Optics EXPRESS

malignant melanoma," Arch. Dermatol. **126**(6), 763–766 (1990).
5. G. Argenziano and H. P. Soyer, "Dermoscopy of pigmented skin lesions--a valuable tool for early diagnosis of melanoma," Lancet Oncol. **2**(7), 443–449 (2001).
6. H. Kittler, H. Pehamberger, K. Wolff, and M. Binder, "Diagnostic accuracy of dermoscopy," Lancet Oncol. **3**(3), 159–165 (2002).
7. K. Hoffmann, J. Jung, S. el Gammal, and P. Altmeyer, "Malignant melanoma in 20-MHz B scan sonography," Dermatology (Basel) **185**(1), 49–55 (1992).
8. C. C. Harland, S. G. Kale, P. Jackson, P. S. Mortimer, and J. C. Bamber, "Differentiation of common benign pigmented skin lesions from melanoma by high-resolution ultrasound," Br. J. Dermatol. **143**(2), 281–289 (2000).
9. C. M. Botar-Jid, R. Cosgarea, S. D. Bolboacă, S. C. Şenilă, L. M. Lenghel, L. Rogojan, and S. M. Dudea, "Assessment of Cutaneous Melanoma by Use of Very- High-Frequency Ultrasound and Real-Time Elastography," AJR Am. J. Roentgenol. **206**(4), 699–704 (2016).
10. C. Botar Jid, S. D. Bolboacă, R. Cosgarea, S. Şenilă, L. Rogojan, M. Lenghel, D. Vasilescu, and S. M. Dudea, "Doppler ultrasound and strain elastography in the assessment of cutaneous melanoma: Preliminary results," Med. Ultrason. **17**(4), 509–514 (2015).
11. T. Hinz, J. Wenzel, and M.-H. Schmid-Wendtner, "Real-time tissue elastography: a helpful tool in the diagnosis of cutaneous melanoma?" J. Am. Acad. Dermatol. **65**(2), 424–426 (2011).
12. M. Elbaum, A. W. Kopf, H. S. Rabinovitz, R. G. Langley, H. Kamino, M. C. Mihm, Jr., A. J. Sober, G. L. Peck, A. Bogdan, D. Gutkowicz-Krusin, M. Greenebaum, S. Keem, M. Oliviero, and S. Wang, "Automatic differentiation of melanoma from melanocytic nevi with multispectral digital dermoscopy: a feasibility study," J. Am. Acad. Dermatol. **44**(2), 207–218 (2001).
13. S. Tomatis, M. Carrara, A. Bono, C. Bartoli, M. Lualdi, G. Tragni, A. Colombo, and R. Marchesini, "Automated melanoma detection with a novel multispectral imaging system: results of a prospective study," Phys. Med. Biol. **50**(8), 1675–1687 (2005).
14. I. Diebele, I. Kuzmina, A. Lihachev, J. Kapostinsh, A. Derjabo, L. Valeine, and J. Spigulis, "Clinical evaluation of melanomas and common nevi by spectral imaging," Biomed. Opt. Express **3**(3), 467–472 (2012).
15. A. Premkumar, F. Marincola, J. Taubenberger, C. Chow, D. Venzon, and D. Schwartzentruber, "Metastatic melanoma: Correlation of MRI characteristics and histopathology," J. Magn. Reson. Imaging **6**(1), 190–194 (1996).
16. H. Yoshioka, T. Kamada, S. Kandatsu, M. Koga, K. Yoshikawa, Y. Matsuoka, J. Mizoe, Y. Itai, and H. Tsujii, "MRI of Mucosal Malignant Melanoma of the Head and Neck," J. Comput. Assist. Tomogr. **22**(3), 492–497 (1998).
17. S. Sigurdsson, P. A. Philipsen, L. K. Hansen, J. Larsen, M. Gniadecka, and H. C. Wulf, "Detection of skin cancer by classification of Raman spectra," IEEE Trans. Biomed. Eng. **51**(10), 1784–1793 (2004).
18. C. A. Lieber, S. K. Majumder, D. Billheimer, D. L. Ellis, and A. Mahadevan-Jansen, "Raman microspectroscopy for skin cancer detection in vitro," J. Biomed. Opt. **13**(2), 024013 (2008).
19. H. Lui, J. Zhao, D. McLean, and H. Zeng, "Real-time Raman spectroscopy for in vivo skin cancer diagnosis," Cancer Res. **72**(10), 2491–2500 (2012).
20. L. Provencher, J. C. Hogue, C. Desbiens, B. Poirier, E. Poirier, D. Boudreau, M. Joyal, C. Diorio, N. Duchesne, and J. Chiquette, "Is clinical breast examination important for breast cancer detection ?" Current Oncology **23**, 332–339 (2016).
21. J. Ophir, I. Céspedes, H. Ponnekanti, Y. Yazdi, and X. Li, "Elastography: A quantitative method for imaging the elasticity of biological tissues," Ultrason. Imaging **13**(2), 111–134 (1991).
22. A. Itoh, E. Ueno, E. Tohno, H. Kamma, H. Takahashi, T. Shiina, M. Yamakawa, and T. Matsumura, "Breast disease: clinical application of US elastography for diagnosis," Radiology **239**(2), 341–350 (2006).
23. D. T. Ginat, S. V. Destounis, R. G. Barr, B. Castaneda, J. G. Strang, and D. J. Rubens, "US elastography of breast and prostate lesions," Radiographics **29**(7), 2007–2016 (2009).
24. J. Guck, S. Schinkinger, B. Lincoln, F. Wottawah, S. Ebert, M. Romeyke, D. Lenz, H. M. Erickson, R. Ananthakrishnan, D. Mitchell, J. Käs, S. Ulvick, and C. Bilby, "Optical deformability as an inherent cell marker for testing malignant transformation and metastatic competence," Biophys. J. **88**(5), 3689–3698 (2005).
25. T. A. Krouskop, T. M. Wheeler, F. Kallel, B. S. Garra, and T. Hall, "Elastic moduli of breast and prostate tissues under compression," Ultrason. Imaging **20**(4), 260–274 (1998).
26. P. Wellman and R. Howe, "Breast tissue stiffness in compression is correlated to histological diagnosis," Harvard BioRobotics Lab. Tech. Rep. 1–15 (1999).
27. S. E. Cross, Y.-S. Jin, J. Rao, and J. K. Gimzewski, "Nanomechanical analysis of cells from cancer patients," Nat. Nanotechnol. **2**(12), 780–783 (2007).
28. S. Suresh, "Nanomedicine: elastic clues in cancer detection," Nat. Nanotechnol. **2**(12), 748–749 (2007).
29. V. Swaminathan, K. Mythreye, E. T. O'Brien, A. Berchuck, G. C. Blobe, and R. Superfine, "Mechanical stiffness grades metastatic potential in patient tumor cells and in cancer cell lines," Cancer Res. **71**(15), 5075–5080 (2011).
30. G. Weder, M. C. Hendriks-Balk, R. Smajda, D. Rimoldi, M. Liley, H. Heinzelmann, A. Meister, and A. Mariotti, "Increased plasticity of the stiffness of melanoma cells correlates with their acquisition of metastatic properties," Nanomedicine (Lond.) **10**(1), 141–148 (2014).
31. M. Sarna, A. Zadlo, A. Pilat, M. Olchawa, P. Gkogkolou, K. Burda, M. Böhm, and T. Sarna, "Nanomechanical analysis of pigmented human melanoma cells," Pigment Cell Melanoma Res. **26**(5), 727–730 (2013).

Biomedical Optics EXPRESS

32. M. Troyanova-Wood, C. Gobbell, Z. Meng, A. A. Gashev, and V. V. Yakovlev, "Optical assessment of changes in mechanical and chemical properties of adipose tissue in diet-induced obese rats," J. Biophotonics **10**(12), 1694–1702 (2017).
33. S. Mattana, M. Mattarelli, L. Urbanelli, K. Sagini, C. Emiliani, M. D. Serra, D. Fioretto, and S. Caponi, "Non-contact mechanical and chemical analysis of single living cells by microspectroscopic techniques," Light Sci. Appl. **7**(2), 17139 (2018).
34. K. Elsayad, S. Werner, M. Gallemí, J. Kong, E. R. Sánchez Guajardo, L. Zhang, Y. Jaillais, T. Greb, and Y. Belkhadir, "Mapping the subcellular mechanical properties of live cells in tissues with fluorescence emission-Brillouin imaging," Sci. Signal. **9**(435), rs5 (2016).
35. F. Palombo, M. Madami, D. Fioretto, J. Nallala, H. Barr, A. David, and N. Stone, "Chemico-mechanical imaging of Barrett's oesophagus," J. Biophotonics **9**(7), 694–700 (2016).
36. R. Schlüßler, S. Möllmert, S. Abuhattum, G. Cojoc, P. Müller, K. Kim, C. Möckel, C. Zimmermann, J. Czarske, and J. Guck, "Mechanical Mapping of Spinal Cord Growth and Repair in Living Zebrafish Larvae by Brillouin Imaging," Biophys. J. **115**(5), 911–923 (2018).
37. S. Mattana, S. Caponi, F. Tamagnini, D. Fioretto, and F. Palombo, "Viscoelasticity of amyloid plaques in transgenic mouse brain studied by Brillouin microspectroscopy and correlative Raman analysis," J. Innov. Opt. Health Sci. **10**(6), 1742001 (2017).
38. G. Antonacci and S. Braakman, "Biomechanics of subcellular structures by non-invasive Brillouin microscopy," Sci. Rep. **6**(1), 37217 (2016).
39. G. S. Figueiredo, S. Bojic, P. Rooney, S. P. Wilshaw, C. J. Connon, R. M. Gouveia, C. Paterson, G. Lepert, H. S. Mudhar, F. C. Figueiredo, and M. Lako, "Gamma-irradiated human amniotic membrane decellularised with sodium dodecyl sulfate is a more efficient substrate for the ex vivo expansion of limbal stem cells," Acta Biomater. **61**, 124–133 (2017).
40. J. N. Webb, J. P. Su, and G. Scarcelli, "Mechanical outcome of accelerated corneal crosslinking evaluated by Brillouin microscopy," J. Cataract Refract. Surg. **43**(11), 1458–1463 (2017).
41. L. E. Millikan, J. L. Boylon, R. R. Hook, and P. J. Manning, "Melanoma in Sinclair swine: a new animal model," J. Invest. Dermatol. **62**(1), 20–30 (1974).
42. M. Troyanova-Wood, Z. Meng, and V. V. Yakovlev, "Elasticity-based identification of tumor margins using Brillouin spectroscopy," Prog. Biomed. Opt. Imaging - Proc. SPIE **9719**, 97190P (2016).
43. Z. Meng, A. J. Traverso, C. W. Ballmann, M. A. Troyanova-Wood, and V. V. Yakovlev, "Seeing cells in a new light: a renaissance of Brillouin spectroscopy," Adv. Opt. Photonics **8**(2), 300 (2016).
44. Z. Meng, A. J. Traverso, and V. V. Yakovlev, "Background clean-up in Brillouin microspectroscopy of scattering medium," Opt. Express **22**(5), 5410–5415 (2014).
45. Z. Meng and V. V. Yakovlev, "Optimizing signal collection efficiency of the VIPA-based Brillouin spectrometer," J. Innov. Opt. Health Sci. **8**(04), 1550021 (2015).
46. Z. Coker, M. Troyanova-Wood, A. J. Traverso, T. Yakupov, Z. N. Utegulov, and V. V. Yakovlev, "Assessing performance of modern Brillouin spectrometers," Opt. Express **26**(3), 2400–2409 (2018).
47. A. J. Traverso, J. V. Thompson, Z. A. Steelman, Z. Meng, M. O. Scully, and V. V. Yakovlev, "Dual Raman-Brillouin Microscope for Chemical and Mechanical Characterization and Imaging," Anal. Chem. **87**(15), 7519–7523 (2015).
48. E. Salomatina, B. Jiang, J. Novak, and A. N. Yaroslavsky, "Optical properties of normal and cancerous human skin in the visible and near-infrared spectral range," J. Biomed. Opt. **11**(6), 064026 (2006).
49. J. N. Bixler, B. H. Hokr, M. L. Denton, G. D. Noojin, D. Aurora, H. T. Beier, R. J. Thomas, B. A. Rockwell, and V. V. Yakovlev, "Assessment of tissue heating under tunable near IR radiation," J. Biomed. Opt. **19**, 070501 (2015).
50. Z. Meng, G. I. Petrov, and V. V. Yakovlev, "Flow cytometry using Brillouin imaging and sensing via time-resolved optical (BISTRO) measurements," Analyst (Lond.) **140**(21), 7160–7164 (2015).
51. C. W. Ballmann, Z. Meng, A. J. Traverso, V. V. Yakovlev, and M. O. Scully, "Impulsive Brillouin microscopy," Optica **4**(1), 124–128 (2017).